Development of a New Force Field for Polynorbornene

S. Ahmed, S. A. Bidstrup, P. A. Kohl, and P. J. Ludovice*

School of Chemical Engineering, Georgia Institute of Technology, Atlanta, Georgia 30332-0100

Received: March 10, 1998

A new force field has been customized for the variation of polynorbornene that contains a bicycloheptane group in the backbone structure. The force field was developed from ab initio density functional theory (DFT), and semiempirical electronic structure calculations for both stereochemical dimers of the 2,3 exo−exo isomer of polynorbornene. The bond length and bond angle parameters were determined using the HF/6-311G** ab initio SCF method. The intrinsic torsion potential was determined using the AM1 semiempirical method and the van der Waals parameters are kept same as in the Dreiding 2.21 force field. Both the bonded and torsional energy functions compared well to DFT calculations. The equilibrium geometry and the torsional energetics of the customized force field differ significantly from generic force fields such as Dreiding. Comparisons to experimentally determined geometry and infrared and Raman spectra were used to determine the optimum ab initio and semiempirical method to use for force field parametrization. The new force field reproduces a polynorbornene dimer crystal structure to a high degree of accuracy.

Introduction

The bicyclic variation of polynorbornene is a polymer currently under investigation for a number of applications, including deep ultraviolet photoresists and interlevel dielectrics in microelectronics applications.[1−6] The 2,3-norbornene monomer undergoes a vinyl-like polymerization that preserves the bicyclic conformation in the backbone of the resulting polymer as seen in Figure 1. This is unlike the commonly employed ring opening metathesis polymerization (ROMP) mechanism which retains only a single ring in the polymer backbone. This polymer is currently being developed by the BFGoodrich Corp. under the trade name Avatrel dielectric polymer. Polynorbornene has excellent dielectric properties and a cost advantage over other materials currently being used as interlevel dielectrics;[1,7] however, the bicyclic backbone structure makes direct experimental characterization of the polymer microstructure with 2-D NMR difficult.[1,8,9] Therefore, we are currently using a combination of molecular mechanics modeling and experiment to characterize the microstructure of this polymer. Molecular mechanics modeling requires an accurate classical force field, and the work presented here is the development of that force field. Ab initio and semiempirical quantum calculations, carried out on the monomer and dimer of poly(norbornene), were used to calculate the bonded and intrinsic torsional potentials. These were combined with nonbonded dispersion parameters from a previously published general force field to produce a classical force field appropriate for the molecular mechanics modeling of the polymer.

Polynorbornene undergoes 2,3 exo−exo enchainment during polymerization, and a variety of properties can be obtained depending on the homogeneous polymerization catalyst system used.[1] We hypothesize that different catalyst systems produce different stereochemistries and this gives rise to different properties. It is presumed that the zirconocene catalyst[10,11] produces the highly stereoregular 2,3-erythro diisotactic polynorbornene because of the intractable polymer produced from this catalyst.

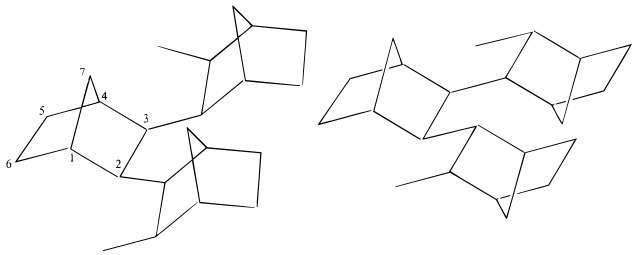

Figure 1. Structure of polynorbornene. The threo disyndiotactic (left) and erythro diisotactic (right) trimers are shown to illustrate possible stereochemical variation.

This polymer does not appear to dissolve in any organic solvents. The stereochemistries produced by other catalyst systems have yet to be determined. The force field described herein has been used to model various stereochemistries of polynorbornene; therefore, energy expressions for both the meso and racemic stereochemical forms of the dimer must be determined (see Figure 1). Note that the polymer chain comprising all meso diads (erythro diisotactic polymers) results in alternating bridging carbons (carbon 7 in Figure 1) when the chain is in the extended cis conformation. Similarly, a chain of all racemic diads (erythro disyndiotactic polymer) results in all the bridging carbons pointing in the same direction in the extended cis conformation. This convention appears to be the opposite for vinyl polymers where an alternating α substituent (i.e., the chlorine in poly(vinyl chloride)) produces a syndiotactic polymer. The stereochemical convention of polynorbornene is derived from that of polysaccharides, and because the polymerization is always in the exo position, both of these isomers are of the erythro variety (as opposed to threo).[12] This force field developed has been shown to accurately model the conformational characteristics of isolated chains as well as bulk polymer systems.[13]

The most critical component of any molecular model is the classical force field used to describe the interatomic interactions in the material.[14] Previous polynorbornene modeling work we have carried out[15] as well as previous work by Heitz and co-

* To whom correspondence should be addressed.

10.1021/jp9814294 CCC: $15.00
Published on Web 11/10/1998

workers[8,9] indicated that commercially available general force fields do not provide a good characterization of the material. This occurs because generic force fields are typically parametrized for simple hydrocarbons and polynorbornene possesses levels of ring strain and hindered torsional rotation higher than in most hydrocarbons. The severe strain in the bicycloheptane repeat unit results in bond lengths and bond angles that deviate significantly from the typical equilibrium values in hydrocarbons. The large bicycloheptane unit in the backbone of polynorbornene produces a very hindered torsional rotation. Rotationally hindered polymer species typically require more elaborate intrinsic torsion potentials[16,17] than the simple two-term trigonometric functions used for vinyl polymers. Since deformation of a polymer segment occurs primarily by rotation around skeletal bonds,[18] an accurate intrinsic torsion potential needs to be determined that accounts for the effect of steric hindrance.

The functional form of the force field terms and the nonbonded parameters were taken from the Dreiding 2.21 force field, which was derived for simple organics.[8,9,15] The functional form of this force field is quite common and contains quadratic bonded terms and Lennard-Jones nonbonded terms. Ab initio calculations are typically performed on the smallest unit representative of the material,[19] and therefore, ab initio calculations were carried out on norbornane to determine the bond stretching and bond bending force constants and equilibrium geometry. To determine the intrinsic torsion potential, modeling of at least a dimer of the material is required. Since numerous nonbonded interactions are included in this torsional rotation energetics, these nonbonded interactions must be included in parametrizing the intrinsic torsional potential. Since no charges are being incorporated into this model, these nonbonded interactions are due to dispersion forces, the origin of which is electron correlation effects. Standard Hartree−Fock ab initio methods do not incorporate the effect of electron correlation without computationally intensive post-SCF processing, such as Møller−Plessett (MP2 or MP4) perturbation theory approaches.[20,21] Limitations on our computational resources precluded the use of ab initio calculations for a fragment of this size with the inclusion of MP2 calculations to account for correlation effects. Therefore, the same procedure was then repeated on a norbornene dimer using semiempirical calculations to determine the proper intramolecular potential. Semiempirical methods were chosen for their computational expediency because the energy at small increments of the torsional angles for two stereoisomers is required. Our computational resources (HP and DEC workstations) were sufficient to calculate the energy using density functional theory (DFT) calculations. However, the DFT calculations were still quite time consuming, requiring a week or more per calculation of a single energy with optimized geometry. The torsional energy function of polynorbornene is more complicated than a simple polymer such as polyethylene. The simple symmetry of polyethylene clearly indicates where the three local minima (180° and two equivalent minima at ±60°) and three barriers (0° and ±120°) are. Since two of the minima and barriers are equivalent, only four energy calculations are required to characterize the torsional energy function of polyethylene. The positions and relative heights of the minima and barriers are the most critical elements of this torsional energy space. However, scores of energy calculations were required for polynorbornene because it lacks this simple symmetry. Therefore, we opted to characterize the torsional energy function using semiempirical calculations and then validate it at a few points using DFT. The non bond van der Waals parameters have been taken from the Dreiding 2.21 force field, because literature suggests that there is little variation in van der Waals parameters for nonpolar materials.[8,9,22] The force fields for both dimer stereochemistries (meso and racemic) were determined.

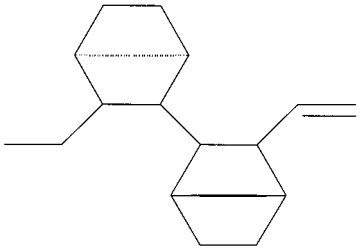

Figure 2. Structure of meso dimer of diethyl derivative of polynorbornene used in WAXD studies.

Methodology

Norbornane monomer geometry was optimized using the ab initio quantum chemistry package Gaussian92/DFT-RevG.4,[23] which performs full geometry optimizations using the Berny optimization algorithm. The Hartree−Fock[20,21] method with the STO-3G[24] and 6-311G**[25] basis sets was employed in this study. The calculations were made in internal coordinates using C1 symmetry. The trade off between computational expediency and accuracy governed the choice of basis sets. While a basis set as large as 6-311G** is not typically required for organic molecules of this size, previous work suggests that the additional polarization functions in this basis are needed for systems with highly strained rings such as the bicycloheptane rings in the system being considered.[21,26] Therefore, we choose this basis set because of the highly strained bicycloheptane rings. A normal-mode frequency analysis was then performed on the geometry-optimized monomer to obtain the infrared and Raman vibrational frequencies. A number of semiempirical methods were also employed to investigate the norbornane monomer geometry using the semiempirical quantum chemistry package MOPAC6.[27] The CNDO,[28,29] MNDO,[30] AM1,[31] and PM3[32] semiempirical methods were employed, and a frequency analysis was performed to determine the infrared vibrational frequency for every semiempirical method. The norbornane dimer was studied using the MNDO and the AM1 semiempirical methods to determine the intrinsic torsion potential. Additional validation of these semiempirical calculations on the meso dimer was performed by calculating a few points on the torsional energy curve using DFT approach. The B3LYP/6-31G* approach was used for these calculations. This approach uses the 6-31G* basis set along with the Becke's three-parameter nonlocal exchange function[33] along with the correlation functionals of Perdew[34] and Lee, Yang, and Parr.[35]

The calculated vibrational frequencies were compared to those determined experimentally from infrared and Raman (only for ab initio calculations) spectra. Optimized bond lengths and bond angles from the ab initio calculations were compared to experimental bond lengths and bond angles determined from wide-angle X-ray diffraction (WAXD) studies on a substituted polynorbornene dimer crystal. The accuracy with which the various methods reproduced these experimental results was used to select the choice of ab initio basis set and the semiempirical method. The meso isomer of the ethylethylene substituted dimer analyzed using WAXD is pictured in Figure 2. An ethyl group is attached to the first bicycloheptane at the 2 position and an ethylene group is attached to the second bicycloheptane at the 3 position. A total of 2016 independent reflections having 2Θ-

TABLE 1: Structure of the New Force Field for Polynorbornene

term	form	explanation
harmonic bond stretch	$(1/2)K_R(R - R_e)^2$	K_R, force constant R, bond length R_e, equilibrium bond length
harmonic angle bend	$(1/2)K_\Theta(\Theta - \Theta_e)^2$	K_Θ, force constant Θ, bond angle Θ_e, equilibrium bond angle
dihedral angle torsion	$\sum(1/2)K_\Phi \cos(n\Phi/2)$	K_Φ, force constant n, periodicity of the potential Φ, torsion angle
van der Waals interactions	$D_o\{[R_o/R]^{12} - 2[R_o/R]^6\}$	D_o, well depth R, separation R_o, equilibrium separation

(Mo Kα) < 45.8° were collected on a computer-controlled Nicolet autodiffractometer using full ω scans and graphite-monochromated Mo Kα radiation. The structure was solved using "direct methods" techniques with the Siemens SHELXTL-PC software package. Raman spectra were measured with a Kaiser Optical Holoprobe 785 Raman microscope using a 785 nm diode laser at a spectral resolution of 4 cm^{-1}. Polarized Raman spectra were collected with the analyzer parallel and perpendicular to the polarizer. IR spectra were measured on a Nicolet 650 spectrometer using a He−Ne laser.

The energy terms comprising the new force field are described in Table 1. These are the same terms employed in the Dreiding 2.21 force field.[36] Given the hydrocarbon structure of polynorbornene, we have omitted the electrostatic interaction in the force field. Note that all the bonded interactions are modeled as independent harmonic terms. This omission of cross terms that include the energetic effects of the bond length on the angle terms assumes that these terms are negligible. This assumption is tested below. The equilibrium bond lengths and bond angles are directly available from quantum mechanical calculations, and the force constants are given by the second derivative of the quantum mechanical energy with respect to internal coordinates as seen in eq 1[22] (where x_i and x_j represent the internal coordinates such as bond lengths or bond angles).

$$k = \frac{\partial^2 E}{\partial x_i \partial x_j}\Big|_e \qquad (1)$$

As mentioned above, the van der Waals parameters utilized in our force field are identical to those used in Dreiding 2.21. Since the charges on the atoms are small, electrostatic interactions are not considered in our force field as a computational expedient.

Results and Discussion

Tables 2 and 3 compare the calculated bond lengths and bond angles from various calculations with the experimental values obtained from WAXD measurements on the substituted dimer of polynorbornene pictured in Figure 2. The 6-311G** basis set was found to provide better comparison to experiment than the other ab initio basis set as well as the semiempirical methods. Therefore, equilibrium bond lengths and angles as well as force constants derived from analytical second derivatives were extracted from the HF/6-311G** calculations. The HF/6-311G** calculations also reproduced the normal-mode frequencies of norbornane better than the other methods. A plot of the normal-mode frequencies obtained from various ab initio and semiempirical calculations vs their experimental counterparts obtained from IR spectroscopy is seen in Figure 3. A similar plot of normal-mode frequencies from both ab initio basis set calculations compared to Raman frequencies is seen in Figure 4. The ab initio frequencies (but not the semiempirical frequencies) were scaled by a factor 0.89 to account for the empirically observed systematic error in HF calculations.[20] The calculated mixed partial derivatives from Equation 1 were all between 1 and 2 orders of magnitude lower than the diagonal second derivatives. This observation justifies the neglect of the cross terms in this force field. Previous force field development work by Heitz and co-workers suggested that HF/STO-3G calculations reproduced the IR frequencies well.[8] However, Heitz et al. considered only the frequencies below 1600 cm^{-1}. Figures 3 and 4 illustrate that while HF/6-311G** calculations are only slightly better that HF/STO-3G calculations in this region, they are much more accurate in the higher frequency region. For this reason the harmonic force constants are derived from the HF/6-311G** calculations. Ordinarily, the C−H stretching frequencies that reside in this higher frequency region (~3000 cm^{-1}) do not have a large effect on the accuracy of the force field because the torsional angle barriers in vinyl polymers are dominated by C−C interactions. However, in this case the highest torsion angle barrier occurs because two pendant hydrogens on the bicycloheptane rings collide with each other during torsion angle rotation. The large perturbation in the C−H bond that results means that the associated C−H bond constants directly effect the torsional barriers. Therefore accurate frequencies in the 3000 cm^{-1} region are important for this system.

The bond stretching and angle bending harmonic force constants for this force field derived from the HF/6-311G** calculations are listed in Table 4. The bond stretch and bond bend force constants were taken from the HF/6-311G** calculation on norbornane with methyl groups on the 2 and 3 carbon positions to simulate the effect of the neighboring carbons. The DFT calculations on dimers below indicated that the force constant parameters were essentially identical to the 2,3-dimethylnorbornane used here, indicating that the presence of a neighboring bicycloheptane group does not affect these bonded parameters. Also listed in this table are the same constants from two generic force fields for organic molecules: Dreiding 2.21 and CHARMM.[37,38] These two generic force fields fail to reflect the geometry and energy of the strained rings present in this system and illustrate the need for a customized force field for this system.

The angle bending force constants are an order of magnitude higher than the respective force constants taken from generic force fields. This is only to be expected since force constants can only be compared across similar compounds[39] and generic force fields are not parametrized for strained rings. These high force constants are due, in part, to the fact that angle bending in norbornane leads to deformation of the strained ring as suggested by previous norbornane calculations.[40] Normally we would expect to see high frequencies associated with these high force constants. However, the angle bending motion is not directly related to the observed frequencies because the angle bending motion is not a normal mode in a bicyclo ring system.[41] A complicated combination of angle bending and angle stretch (ring deformation) is what is experimentally observable and therefore the high force constants do not directly translate into extremely high frequencies because of the mixed nature of the ring deformation modes. We found that other cyclic compounds

TABLE 2: Comparison of Bond Lengths Obtained from Calculations and Experiment

equilib bond length between atoms	HF/6-311G**	HF/STO-3G	PM3	AM1	MNDO	CNDO	expt
{C2−C3}, {C5−C6}	1.557	1.559	1.543	1.541	1.557	1.541	1.563
{C1−C7}, {C4−C7}	1.537	1.545	1.545	1.551	1.562	1.551	1.523
{C1−C2}, {C3−C4}	1.540	1.551	1.542	1.542	1.561	1.542	1.536
{C4−C5}, {C1−C6}	1.540	1.551	1.542	1.542	1.561	1.542	1.536

TABLE 3: Comparison of Bond Angles Obtained from Calculations and Experiment

equilib bond angle between atoms	HF/6-311G**	HF/STO-3G	PM3	AM1	MNDO	CNDO	expt
{C1−C2−C3}, {C2−C3−C4}	103.1	103.2	103.5	103.8	103.2	103.8	101.9
{C4−C5−C6}, {C5−C6−C1}	103.1	103.2	103.5	103.8	103.2	103.8	102.8
{C3−C4−C7}, {C5−C4−C7}	101.5	101.5	101.4	101.3	101.4	101.3	101.7
{C2−C1−C7}, {C6−C1−C7}	101.5	101.5	101.4	101.3	101.4	101.3	102.2
{C1−C7−C4}	94.4	94.3	94.2	94.3	93.1	94.3	94.0

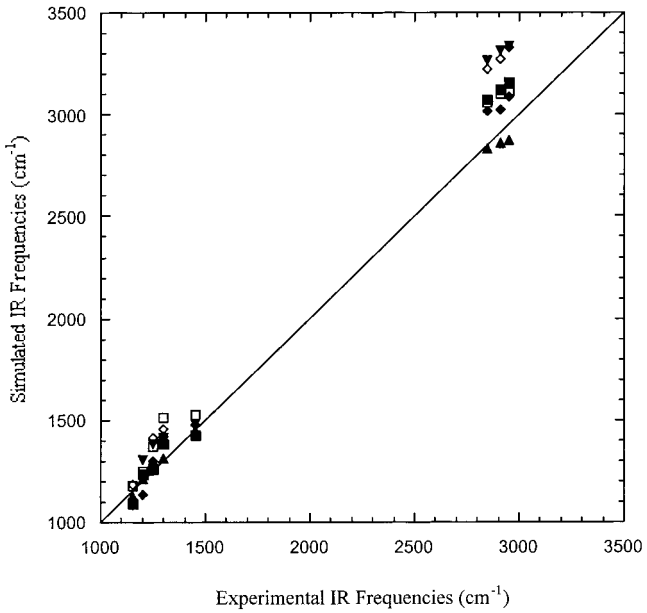

Figure 3. Comparison of IR frequencies from different simulation methods to experiment. Proximity to the diagonal line indicates better comparison to experiment. The Hartree−Fock frequencies (HF/6-311G*, HF/STO-3G) have been scaled by a factor of 0.89. (◆) HF/6-311G**, (◇) HF/STO-3G, (▼) AM1, (▲) MNDO, (■) PM3, (□)-DFT/B3LYP. HF/6-311G** compares best with experiment, and AM1 compare best among the semiempirical methods.

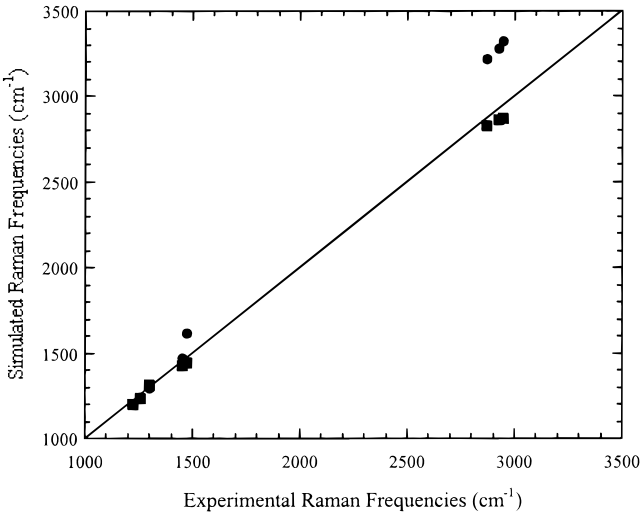

Figure 4. Comparison of Raman frequencies from different simulation methods to experiment. Proximity to the diagonal line indicates better comparison to experiment. The simulation frequencies have been scaled by a factor of 0.89. (■) HF/6-311G** and (●) HF/STO-3G. HF/6-311G** compares best with experiment.

such as cyclobutane also give these high force constants for the ring angle bending mode. However, the ring strain can be expressed as any combination of bond stretch and bond bend motions,[42,43] and we chose the internal deformation modes that are generally used in most force fields for convenience. These high force constants are not dependent upon the basis set used in the calculation since our results for the 6-311G**, STO-3G basis sets and separate calculations using the 6-31G*[44] basis set all give very similar internal force constants.

Although the ring strain in the bicycloheptane ring is partly responsible for the high angle force constants produced from the ab initio calculations, there is still some ambiguity regarding these high values. In Gaussian as well as other ab initio quantum packages, the internal coordinate force constants can be derived from the Cartesian force constants via a chain rule derivative expansion that employs the derivative of the Cartesian coordinate with respect to the internal coordinate. Unfortunately, the ring structure makes the calculation of this derivative ambiguous because one needs to assume some symmetry of motion. Therefore, the values reported in Table 5 are the results of an assumed symmetry. The effect of this assumption is currently under investigation and we are in the process of fitting the internal mode force constants such that they optimally reproduce the Cartesian force constants. However, for most polymer simulations the high angle bending constants reported in Table 5 should not significantly affect the results. The force field reported here models the bicycloheptane ring as fairly rigid, but the torsional energetics, which are critical to the conformational description of the polymer, are reasonable. Note the C−C−H angle constants are not significantly inflated and these would have the most pronounced effect on the conformational behavior through the hydrogen collisions during backbone rotaions.

The change in energy as a function of the rotation of a backbone torsion angle is composed of two components: (i) the interatomic interaction of atoms offset by three atoms or more along the backbone (1−4 interaction) and (ii) the deformation of the bonding orbitals along the backbone. The first component is accounted for by the Lennard-Jones interactions of all backbone atoms. The second component is an explicit function of the torsion angle, called the intrinsic torsional potential. The intrinsic torsional potential is an analytical function added to the force field such that the sum of the Lennard-Jones interactions is a function of torsional angle and it reproduces the torsional energetics, which in this case were derived from semiempirical calculations. Since energy from semiempirical calculations was used to characterize the torsional energetics, the intrinsic torsional potential was obtained by subtracting the aforementioned backbone Lennard-Jones interac-

TABLE 4: Comparison of Bond Stretch Force Constants Obtained from ab Initio Calculations to Dreiding 2.21 and CHARMM 3.03

bond stretch force constants between atoms	HF/6-311G** (kcal/(mol Å^2))	Dreiding 2.21 force field (kcal/(mol Å^2))	CHARMM 3.03 force field (kcal/(mol Å^2))
{C2−C3}, {C5−C6}	1802.23	700.00	536.00
{C1−C7}, {C4−C7}	811.00	700.00	536.00
{C1−C2}, {C3−C4}	803.00	700.00	536.00
{C4−C5}, {C1−6}	803.00	700.00	536.00
C−H average	810.00	700.00	300.00

TABLE 5: Comparison of Bond Bend Force Constants Obtained from ab Initio Calculations to Dreiding 2.21 and CHARMM 3.03

bond bend force constants between atoms	HF/6-311G** (kcal/(mol rad^2))	Dreiding 2.21 force field (kcal/(mol rad^2))	CHARMM 3.03 force field (kcal/(mol Å^2))
{C1−C2−C3}, {C2−C3−C4}	5485.00	100.00	116.7
{C4−C5−C6}, {C5−C6−C1}	4550.00	100.00	116.7
{C3−C4−C7}, {C2−C1−C7}	1105.00	100.00	116.7
{C5−C4−C7}, {C6−C1−C7}	1105.00	100.00	116.7
{C1−C7−C4}	800.00	100.00	116.7
C−C−H average	155.00	100.00	40.00

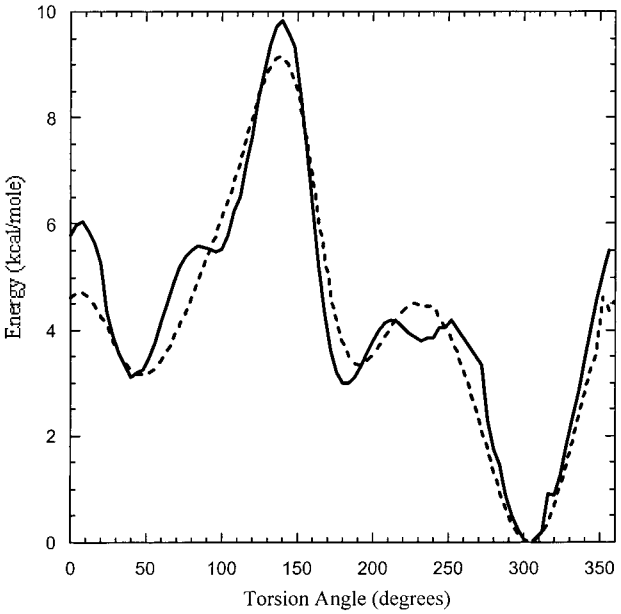

Figure 5. Racemic dimer. Comparison of AM1 and MNDO torsion potential results. Solid line represents AM1 results and dashed line represents MNDO results.

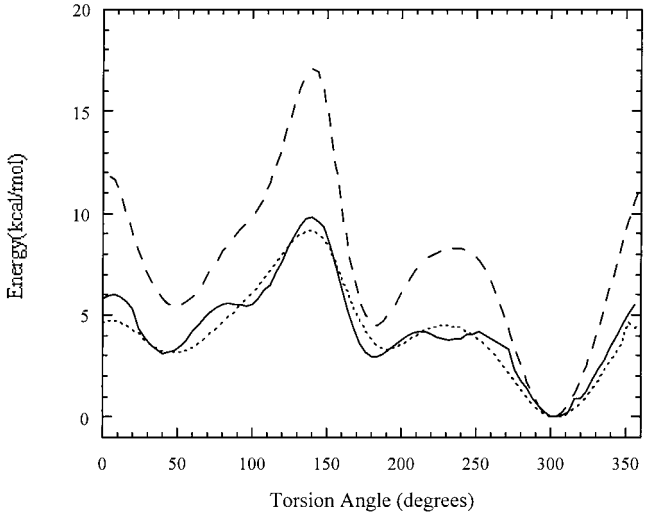

Figure 6. Comparison between AM1 and Dreiding 2.21 force field for the intrinsic torsion potential. Racemic dimer. Solid line represents AM1 results, dotted line represents MNDO results and the dashed line represents Dreiding 2.21 force field results.

tions from the energy function obtained from the semiempirical calculations. Of all the semiempirical methods considered above the AM1 method has been generally found to be the most accurate for studying dihedral angles.[45] Although most of the semiempirical methods reproduced the equilibrium geometry to about the same degree of accuracy (see Tables 2 and 3), the AM1 method produced the most accurate force constant estimates as seen in Figure 3. Therefore, to determine the intrinsic torsion potential the AM1 semiempirical method was employed. For comparison, an MNDO simulation was also undertaken which produced results that were very similar. Comparisons of the results from these two methods are seen in Figure 5 for the racemic dimer.

The results from the two calculations are also in general agreement with the results from an STO-3G calculation by Heitz and co-workers for the racemic diad.[9] Heitz and co-workers had characterized only the racemic diad, but found the same deviation from the Dreiding force field as exhibited in Figure 6. However, they concluded that the similar shape of the curves between their results and the Dreiding force field justified the use of the Dreiding force field for polynorbornene.[8,9] We take issue with this conclusion as both the torsional barriers and the difference in the local minima differ significantly from the Dreiding force field. The two local energy minima are approximately 1.5 and 2 kcal/mol higher that the lowest minimum in the torsional energy plotted in Figure 6. This could significantly affect the conformation of the polymer at room temperature. The flat region between 200° and 250° could be populated in a bulk polymer if the MNDO, AM1, or Heitz's STO-3G results are used, but not if the Dreiding force field was used. The difference is even more significant if properties that depend on the barrier heights, such as the glass transition temperature (T_g) which is of great interest for many polynorbornene applications, are to be calculated. Recently, Gee and Boyd simulated polyethylene molecules with various intrinsic torsional potentials using molecular dynamics (MD) and found a relationship between the torsional energy barriers and T_g.[46] Since the onset of molecular motion occurs at T_g, it is to be expected that the highest torsional barrier is related to T_g. We plotted the simulated T_g vs the highest torsional barrier (difference between the maximum and minimum in the torsional energy function) for Boyd and Gee's simulations. This resulted in a linear relationship ($R = 0.950$) with a slope of 38.7 °C/(kcal/mol). This suggests that every increase in the maximum

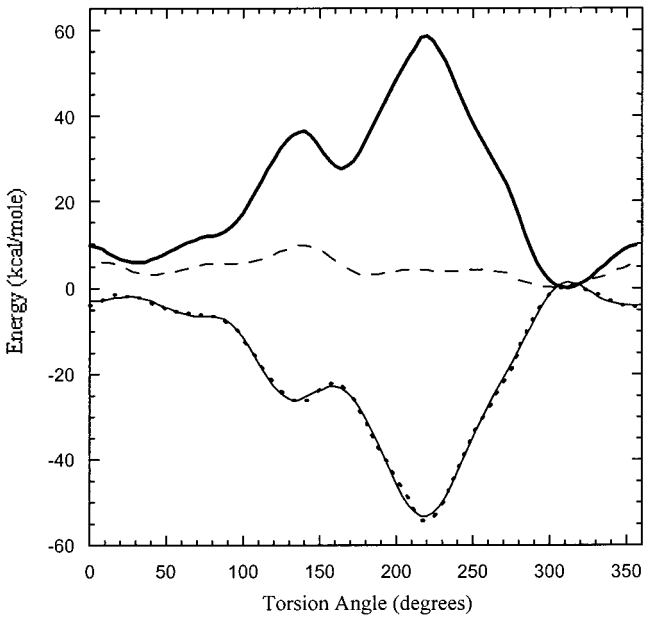

Figure 7. Racemic dimer. The force field with the corrected bond stretch and angle bend terms, but without an intrinsic torsion term is compared against AM1 values. The difference between the two is then fitted as an intrinsic torsion to the force field. The bold solid line represents the force field without the intrinsic torsion term, the dashed line represents AM1 results, the dotted line represents the difference between the two, and the solid line represents the fitted intrinsic torsion term.

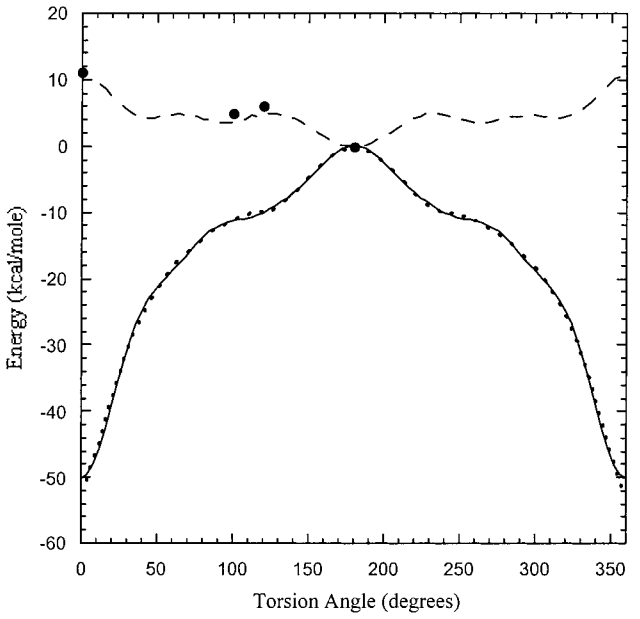

Figure 8. Meso dimer. The force field with the corrected bond stretch and angle bend terms, but without an intrinsic torsion term is compared against AM1 values. The difference between the two is then fitted as an intrinsic torsion to the force field. The dashed line represents AM1 results, the dotted line represents the difference between the AM1 results and the force field without the intrinsic torsion term, and the solid line represents the fitted intrinsic torsion term. The solid circles represent DFT/B3LYP results.

torsional barrier by 1 kcal/mol increases T_g by 38.7 °C independent of the surrounding intermolecular contributions. Therefore, if we assume the intermolecular barriers are independent of the intramolecular torsional barrier then this relationship derived from polyethylene would provide an estimate of the change in the simulated T_g that might result in a drastically different torsional energy barrier. As seen in Figure 6, this maximum torsional energy barrier from the Dreiding force field is over 7 kcal/mol higher than that obtained from the semiempirical calculations. This difference is also observed in the barrier obtained by Heitz in the STO-3G calculations. This difference in the torsional barrier corresponds to a difference in T_g of approximately 270 °C.

It is likely that the differences in the torsional energy function may contribute to differences in polymer structure, and polymer simulations using the functions developed here are in progress to determine this.[13] The force field with the correct bond stretch and bond bend parameters was then corrected to reflect the correct barriers to rotation. The AM1 results along with the energetic variation due to only the backbone Lennard-Jones interaction, and the resulting intrinsic torsional potential are pictured in Figure 7 and Figure 8 for the racemic and meso diads, respectively. The torsion angle potentials were fit to a 15-term cosine series given in Table 1. The coefficients are listed in Table 6. Typically, polymer intrinsic torsional potentials can be fit to a cosine series containing from two to six terms, but the complex nature of polynorbornene requires a more complex function for the racemic diad.

The data in Tables 2−6 along with the Lennard-Jones parameters from the original Dreiding force field comprise the new force field for polynorbornene. The only true validation of this force field is the accurate calculation of polymer properties. Bulk amorphous conformations of polynorbornene as a function of molecular weight compared well to experimental intrinsic viscosity measurements.[13] As an additional direct test of the force field, we compared the simulated crystal structure

TABLE 6: Coefficients of the 15-Term Torsion Potential for the Meso and Racemic Dimers[a]

period (n)	racemic dimer	meso dimer (6 term)	meso dimer
0	−17.9644	−16.937	−16.9261
1	3.8744		0.0144
2	19.6167	−17.353	−17.3322
3	−8.1633		0.0011
4	−1.2956	−5.483	−5.4622
5	5.2633		0.0089
6	−5.2067	−5.452	−5.4311
7	−0.5244		0.0078
8	2.2667	−1.616	−1.5944
9	−0.5033		−0.0056
10	−1.4333	−1.876	−1.8544
11	−0.9989		−0.0033
12	0.0711	−1.048	−1.0267
13	−0.5911		0.0189
14	0.4289		−0.5211

[a] The equation for dihedral angle torsion is presented in Table 1. A six-term series is sufficient to reproduce the meso dimer torsional potential, but 15 terms are required for the racemic dimer.

of the ethylethylene-substituted meso dimer pictured in Figure 10 to its experimentally measured structure. The force constants for the ethyl and ethylene groups were taken from the Dreiding 2.21 force field, whereas the equilibrium geometry for the ethylene groups was computed using HF/6-311G** ab initio calculation on the norbornane dimer with ethyl terminal groups. Following minimization to a root mean square (rms) force of 0.01 kcal/(Å mol), the simulated crystal WAXD pattern compared well with the experimentally determined one (Figure 9). The WAXD pattern was calculated using CERIUS2 (version 3.5) from Molecular Simulations Inc.[47] The rms deviation in the position of carbon atoms was 0.1959 Å, which is good considering the size of the crystal cell. For comparison, an identical simulation using the Dreiding 2.21 force field gave a rms deviation of 0.2583 Å in the positions of carbon atoms.

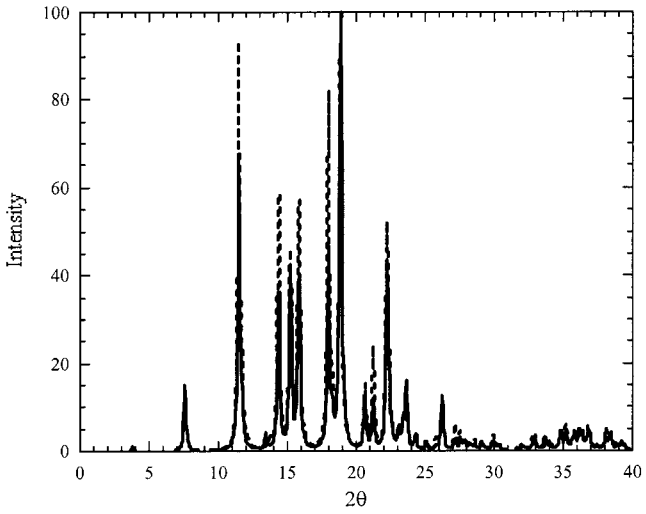

Figure 9. Simulated X-ray crystal diffraction spectra of 2,3 erythro-diisotactic polynorbornene dimers with ethylene terminal groups is compared to experiment. The experimental spectra was reconstructed using 3D anisotropic Debye−Waller factors. The dashed lines represent experimental data and the solid lines represent simulation results.

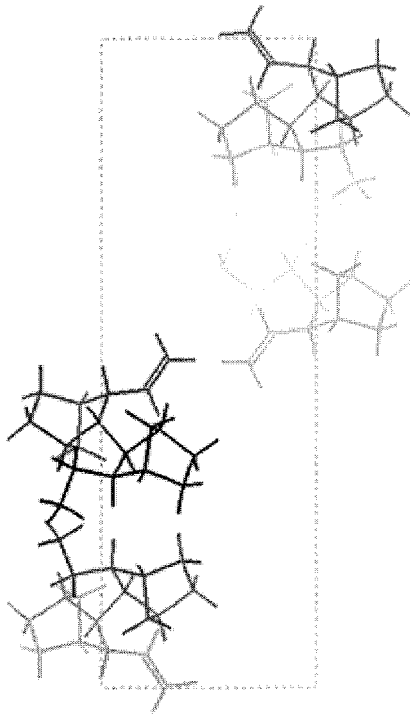

Figure 10. Crystal cell that was simulated. Crystal system was monoclinic with the space group $P2_1/n$. Lattice constants were $a = 7.947$ Å, $b = 23.270$ Å, $c = 8.248$ Å, $\alpha = 90.00°$, $\beta = 104.29°$, $\gamma = 90.00°$. The cell volume is 1478 Å^3 and the cell density is 1.098 g cm^{-3}. There are 18 carbon and 28 hydrogen atoms in the crystal cell. There are no charges on the atoms. The cell parameters were held constant during minimization.

Using ab initio and semiempirical electronic structure calculations, a new classical force field for polynorbornene was derived. This force field differs significantly from generic force fields such as Dreiding 2.21 due, in part, to the large degree of ring strain in polynorborene. The equilibrium structure produced using this force field accurately reproduced the crystal structure of a substituted meso dimer crystal. Derived force constants also reproduced the infrared and Raman spectra over a wide range of frequencies. This force field is currently in use and has accurately reproduced structure−property relationships for polynorbornene.[13] These high values of the angle bending constants are partly due to ring strain. However, the presence of rings in the repeat unit makes the direct calculation of force constants in internal coordinates from the Cartesian Hessian somewhat problematic. Even if these force constants are higher than they should be, this should not significantly affect the polymer conformation. The exact origin of these high force constants is currently under investigation.

Acknowledgment. We gratefully acknowledge financial support from the ONR funded Molecular Design Institute at Georgia Tech, the Georgia Tech Polymer Program Associates, and the BFGoodrich Corp. The assistance of Drs. Robert Schick and Brian Goodall and their colleagues from the BF Goodrich Corp. is gratefully acknowledged. We also appreciate the assistance of Professor Prashant Desai from Georgia Tech for the Raman spectroscopy measurements, and helpful discussions with Dr. Richard Jaffe of the NASA−Ames Research Center.

References and Notes

(1) Grove, N. R.; Zhao, Q.; Kohl, P. A.; Bidstrup-Allen, S. A.; Shick, R. A.; Goodall, B. L.; McIntosh, L. H.; Jayaraman, S. *Adv. Microelectron.* **1996**, *23*, 16.

(2) Grove, N. R.; Zhao, Q.; Kohl, P. A.; Bidstrup-Allen, S. A.; Shick, R. A.; Goodall, B. L.; McIntosh, L. H.; Jayaraman, S. *IEEE Multichip Module Conf. Proc.* **1997**.

(3) *HOECHST Magazin Future IV* **1995**, 52.

(4) *HOECHST Magazin Future IV Special Science 1* **1995**, 32.

(5) Osan, F.; Hatke, W.; Helmer-Metzmann, F.; Jacobs, A.; Land, H. T.; Weller, T. *Cycloolefinic Copolymers*; Lecture Bayreuth Polymer Symposium, 1995.

(6) Czornyj, G.; Asano, M.; Beliveau, R. L.; Garrou, P.; Hiramoto, H.; Ikeda, A.; Kreuz, J. A.; Rohde, O. In *Microelectronics Packaging Handbook Part II*; Tummala, R. R., Rymaszewski, E. J., Klopfenstein, A. G., Eds.; Chapman & Hall: New York, 1997; p 548.

(7) Pierce, D. W.; Realff, M. J. *Comput. Chem. Eng. Suppl Part B* **1996**, *20*, S1307.

(8) Haselwander, T. F. A.; Heitz, W.; Krugel, S. A.; Wendorff, J. H. *Macromolecules* **1997**, *30*, 5345.

(9) Haselwander, T. F. A.; Heitz, W.; Krugel, S. A.; Wendorff, J. H. *Macromol. Chem. Phys.* **1996**, *197*, 3435.

(10) Arndt, M.; Engehausen, R.; Kaminsky, W.; Zoumis, K. *J. Mol. Catal. A: Chem.* **1995**, *101*, 171.

(11) Kaminsky, W.; Noll, A. *Polym. Bull.* **1993**, *31*, 175.

(12) Arndt, M.; Kaminsky, W. *Macromol. Symp.* **1995**, *97*, 225−246.

(13) Ahmed, S.; Allen, S. A.; Kohl, P.; Ludovice, P. J. *Macromol. Chem.: Macromol. Symp.*, in press.

(14) Allinger, L. A.; Burkert, U. *Molecular Mechanics*; American Chemical Society: Washington, DC, 1982.

(15) Ahmed, S. A.; Allen, S. A.; Kohl, P.; Ludovice, P. J. "Computer Simulation of Polymers for Dielectric Applications". *Proc. Soc. Plast. Eng ANTEC Meeting*, **1996**, *2*, 2179.

(16) Hutnik, M.; Suter, U. W. *Polym. Prepr.* **1987**, *28*, 293.

(17) Hutnik, M.; Argon, A.; Suter, U. W. *Macromolecules* **1991**, *24*, 5956.

(18) Gentile, F. T.; Suter, U. W. In *Encyclopedia of Polymer Science*; Haanseen, P., Kramer, E., Eds.; VCH Publishers: New York, 1993.

(19) Galiatsatos, V. In *Reviews in Computational Chemistry*; Lipkowitz, K. B., Boyd, D. B., Eds.; VCH Publishers: New York, 1995; Vol. 6, p 149.

(20) Foresman, J. B.; Frisch, A. *Exploring Chemistry with Electronic Structure Methods: A Guide to Using Gaussian*; Gaussian: Pittsburgh, PA, 1993.

(21) Hehre, W. J.; Radom, L.; Schleyer, P.; Pople, J. A. *Ab Initio Molecular Orbital Theory*; John Wiley: New York, 1986.

(22) Dinur, U.; Hagler, A. T. In *Reviews in Computational Chemistry*; Lipkowitz, K. B., Boyd, D. B., Eds.; VCH Publishers: New York, 1991; Vo. 2, p 99.

(23) *Gaussian 92/DFT, Revision G.4*; Frisch, M. J.; Trucks, G. W.; Schlegel, H. B.; Gill, P. M. W.; Johnson, B. G.; Wong, M. W.; Foresman, J. B.; Robb, M. A.; Head-Gordon, M.; Replogle, E. S.; Gomperts, R.; Andres, J. L.; Raghavachari, K.; Binkley, J. S.; Gonzalez, C.; Martin, R. L.; Fox, D. J.; Defrees, D. J.; Baker, J.; Stewart, J. J. P.; Pople, J. A. Gaussian: Pittsburgh, PA, 1993.

(24) Hehre, W. J.; Stewart, R. F.; Pople, J. A. *J. Chem. Phys.* **1969**, *51*, 2657.

(25) Krishnan, R.; Frisch, M. J.; Pople, J. A. *J. Chem. Phys.* **1980**, *72*, 4244.
(26) Fogarasi, G.; Pulay, P. *Vibr. Spectra Struct.* **1985**, *14*, 125.
(27) Stewart, J. J. P. Frank J. Seiler Research Laboratory, United States Air Force Academy, CO 80840, 1990.
(28) Pople, J. A.; Santry, D. P.; Segal, G. A. *J. Chem. Phys.* **1965**, *43*, S129.
(29) Pople, J. A.; Segal, G. A. *J. Chem. Phys.* **1965**, *43*, S136.
(30) Dewar, M. J. S.; Thiel, W. *J. Am. Chem. Soc.* **1977**, *99*, 4899.
(31) Dewar, M. J. S.; Zoebisch, E. G.; Healy, E. F.; Stewart, J. J. *J. Am. Chem. Soc.* **1985**, *107*, 3902.
(32) Stewart, J. J. P. *J. Comput. Chem.* **1989**, *10*, 209.
(33) Becke, A. D. *Phys. Rev. A.* **1988**, *38*, 3098.
(34) Perdew, J. P. *Electronic Structure of Solids*; Siesche, P., Eschring, H., Eds.; Akademie Verlag: Berlin, 1991; Vol. 4.
(35) Lee, C.; Yang, W.; Parr, R. G. *Phys. Rev. B* **1988**, *37*, 785.
(36) Mayo, S. L.; Olafson, B. D.; Goddard, W. A. *J. Phys. Chem.* **1990**, *32*, 8897.
(37) Brooks, B. R.; Bruccoleri, R. E.; Olafson, B. D.; States, D. J.; Swaminathan, S.; Karplus, M. *J. Comput. Chem.* **1983**, *4*, 187.
(38) *Quanta Version 3.3 Parameter Handbook*; Molecular Simulations: Waltham, MA, 1992.
(39) Wiberg, K. B.; Dailey, W. P.; Walker, F. H.; Waddell, S. T.; Crocker, L. S.; Newton, M. *J. Am. Chem. Soc.* **1985**, *107*, 7247.
(40) Shaw, R. A.; Castro, C.; Dutler, R.; Rauk, A.; Wieser, H. *J. Chem. Phys.* **1988**, *89*, 716.
(41) Pulay, P.; Fogarasi, G.; Pang, F.; Boggs, J. E. *J. Am. Chem. Soc.* **1979**, *101*, 2550.
(42) Wiberg, K. B.; Rosenberg, R. E. *J. Phys. Chem.* **1992**, *96*, 8282.
(43) Wiberg, K. B.; Rosenberg, R. E.; Waddell, S. T. *J. Phys. Chem.* **1992**, *96*, 8294.
(44) Jaffe, R. NASA-Ames Research Center, Moffett Field, CA (unpublished results).
(45) Stewart, J. J. P. In *Reviews in Computational Chemistry*; Lipkowitz, K. B., Boyd, D. B., Eds.; VCH Publishers: New York, 1990; Vol. 1, p 45.
(46) Gee, R.; Boyd, R. *Comput. Theor. Polym. Sci.* **1998**, *8*, 93−98.
(47) Molecular Simulations Inc., 9685 Scranton Rd., San Diego, CA 92121.